Nonlinear holographic crystallography

X. Chen and D. K. Saldin
Department of Physics and Laboratory for Surface Studies, University of Wisconsin-Milwaukee, P.O. Box 413, Milwaukee, Wisconsin 53201
(Received 14 July 1994)

We point out the limitations of linear computer reconstruction algorithms employed previously in holographic crystallography. We show that many of the undesirable artifacts on prior holographic reconstruction of atom positions from point-source diffraction patterns may be traced directly to the nonlinear object-wave terms neglected in traditional holography. This problem is particularly severe in the so-called forward-scattering geometry, represented by, e.g., a subsurface B-atom emitter in the Si(111)-$\sqrt{3}\times\sqrt{3}$ B surface. We show that, even in this case, unlike the prior linear schemes, the nonlinear algorithm "atomic-position recovery by iterative optimization of reconstructed intensities" is capable of recovering a very accurate, artifact-free and twin-image-free, three-dimensional reconstruction of the positions of nearby scattering atoms even for a *single* diffraction pattern.

I. INTRODUCTION

Direct methods in crystallography[1] bring advantages of both elegance and speed to the problem of recovering relative atom positions from diffraction data. The paradigm of using ideas[2] derived from holography[3] to solve crystallographic problems in photoelectron diffraction (PD) (Ref. 4) and low-energy electron diffraction (LEED) (Ref. 5) have been pursued vigorously in recent years.[6] The methodology is the use of a computer algorithm to reconstruct, directly from a diffraction pattern, a three-dimensional real-space intensity distribution mapping the relative positions of atoms in a sample. Although the early work was very promising, the reconstructed intensities were sometimes marred by holographic twin images and unsightly artifacts away from true atom positions,[7] which cast some doubt on the use of such methods to solve completely unknown crystallographic structures.

An attempt has been made to overcome these problems by increasing the pool of available experimental data, for instance, by simultaneously using information from a set of diffraction patterns due to radiation of different wavelengths from the same sample.[8] A generalization of the reconstruction algorithm for such combined datasets has been shown to be capable of generating real-space intensities much less disfigured by artifacts and twin images. However, the collection of a set of diffraction patterns from radiation of several different wavelengths is quite an onerous task, and may not even be possible in, e.g., Auger-electron diffraction, where the wavelengths are determined by differences between atomic energy levels, and are not therefore variable at will. In holographic LEED,[5,9] methods have recently been suggested[10,11] which use data from not only different wavelengths, but also different directions of incidence of the electron beam on a sample, a procedure which has some analogies with tomography, and which may increase the required dataset by a further order of magnitude for an unknown structure.

In this paper we take the different approach of asking whether a more sophisticated algorithm might enable the reconstruction of a three-dimensional map of the positions of atomic scatterers relative to an emitter, free from artifacts and twin images, even from the data of a *single* diffraction pattern. That is, we put the onus more on the theorist than on the experimentalist to recover a higher-quality holographic reconstruction from a limited dataset.

II. THE AIM OF HOLOGRAPHIC CRYSTALLOGRAPHY

The most general definition of a hologram[3] is an intensity distribution $H(\mathbf{k})$ measured over some domain spanned by a coordinate $\mathbf{k}$, and formed by the interference between some known reference wavefront $R(\mathbf{k})$ and some unknown object wave $O(\mathbf{k})$. Thus

$$H(\mathbf{k})=|R(\mathbf{k})|^2+\mathbf{R}(\mathbf{k})O^*(\mathbf{k})+R^*(\mathbf{k})O(\mathbf{k})+|O(\mathbf{k})|^2 . \quad (1)$$

The science of holography was born when Gabor[3] discovered a technique for recovering the unknown object wave $O(\mathbf{k})$ from a measured hologram $H(\mathbf{k})$ and knowledge of the form of the reference wave $R(\mathbf{k})$.

In holographic crystallography the hologram is some measured diffraction pattern, and the aim is to go beyond the recovery of an object wavefield O, usually a wave scattered by an atom, to reconstruct the position of the source of the scattered wave, namely the scattering atom, relative to the source of the reference wave R, usually another atom in the sample. If the reference-wave sources are a set of identical atoms which emit Auger electrons or photoelectrons, a diffuse diffraction pattern may be formed which is characteristic of the emitting atom and the local cluster of atomic scatterers in its vicinity.[6] For emitters consisting of atomic adsorbates on a surface, the cluster of scatterers will be the local substrate atoms closest to each adsorbate. In the cases of Auger-electron and photoelectron diffraction, since each

emission process is essentially independent of all the others, a diffuse diffraction pattern is formed even in the presence of long-range spatial order among the emitters. In the case of the "diffuse low-energy electron-diffraction" (diffuse LEED or DLEED) pattern,[12,5] formed when a beam of low-energy electrons are directed from an *external* source onto a crystal surface containing adsorbates, a similar diffuse diffraction pattern is formed in the presence of lattice-gas *disorder* of the adsorbates with respect the substrate.

In all these cases, the far-field variation of the object wave $O(\mathbf{k})$ may be written

$$O(\mathbf{k})=\sum_i S(\mathbf{r}_i,\mathbf{k}) , \tag{2}$$

where $S(\mathbf{r}_i,\mathbf{k})$ represents the wave field emerging from a scattering atom at position $\mathbf{r}_i$ after multiple scattering from all its neighbors, and $\mathbf{k}$ is the far-field wave vector of an electron giving rise to the intensity $H(\mathbf{k})$. The distribution of $H(\mathbf{k})$ may be sampled for different values of both the direction and magnitude of the wave vector $\mathbf{k}$. In mathematical terms, the aim of holographic crystallography is to devise some kind of computer algorithm which would recover, as accurately as possible, the atomic positions $\mathbf{r}_j$ from the measured data $H(\mathbf{k})$.

III. LINEAR RECONSTRUCTION SCHEMES—e.g., THE BARTON AND SWIFT ALGORITHMS

An approach which has been tried is to perform an integral of the form

$$A(\mathbf{r})=\int H(\mathbf{k})K(\mathbf{r},\mathbf{k})d\mathbf{k} , \tag{3}$$

which can be regarded as a sum of four terms:

$$A_1(\mathbf{r})=\int |R(\mathbf{k})|^2K(\mathbf{r},\mathbf{k})d\mathbf{k} , \tag{4}$$

$$A_2(\mathbf{r})=\int R(\mathbf{k})O^*(\mathbf{k})K(\mathbf{r},\mathbf{k})d\mathbf{k} , \tag{5}$$

$$A_3(\mathbf{r})=\int R^*(\mathbf{k})O(\mathbf{k})K(\mathbf{r},\mathbf{k})d\mathbf{k} , \tag{6}$$

$$A_4(\mathbf{r})=\int |O(\mathbf{k})|^2K(\mathbf{r},\mathbf{k})d\mathbf{k}, \tag{7}$$

from the four terms in (1). If a kernel $K(\mathbf{r},\mathbf{k})$ is chosen such that

$$\int R(\mathbf{k})S^*(\mathbf{r}_i,\mathbf{k})K(\mathbf{r},\mathbf{k})d\mathbf{k}\simeq\delta(\mathbf{r}-\mathbf{r}_i) \tag{8}$$

the function (5) would pick out the positions of the scatterers, since then

$$A_2(\mathbf{r})\simeq\sum_i\delta(\mathbf{r}-\mathbf{r}_i) . \tag{9}$$

The relation (8) essentially represents an orthogonality condition which would be expected to be exact only if the integral is carried out over an infinite domain. In practice, of course, measured data of $H(\mathbf{k})$ is finite, and the best that can be hoped for is that $A_2(\mathbf{r})$ is strongly peaked around the positions $\mathbf{r}=\mathbf{r}_i$, with a peak width inversely proportional to the range of the variable $\mathbf{k}$.

Various approximations to $K(\mathbf{r},\mathbf{k})$ have been suggested. For example, Barton's[4,8] most general kernel takes the form

$$K(\mathbf{r},\mathbf{k})=e^{i(kr-\mathbf{k}\cdot\mathbf{r})} , \tag{10}$$

while (for an s-wave emitter) a more accurate scattered-wave included Fourier-transform (SWIFT) kernel[13] may be written

$$K(\mathbf{r},\mathbf{k})=re^{i(kr-\mathbf{k}\cdot\mathbf{r})}|f_{\mathrm{SW}}^{(0)}(\mathbf{k},\mathbf{r})|/f_{\mathrm{SW}}^{(0)}(\mathbf{k},\mathbf{r}) , \tag{11}$$

where $f_{\mathrm{SW}}^{(0)}(\mathbf{k},\mathbf{r})$ is the appropriate spherical-wave scattering factor[13] for an atom at position $\mathbf{r}$ relative to the emitter. This kernel differs slightly from that of Ref. 13 in the existence in the numerator of the modulus of the scattering factor. This extra factor is inserted to compensate for the possibility that the denominator may vanish at certain values of its argument.

If the peaks in $A_2(\mathbf{r})$ at the atom positions $\mathbf{r}_i$ dominate over the other more diffuse contributions to $A(\mathbf{r})$, the dominant features of the function

$$I(\mathbf{r})=|A(\mathbf{r})|^2 \tag{12}$$

would be expected to reveal the distribution of atoms around the emitter. The problem is that there is no way *a priori* to be sure that the terms A_1, A_3, and A_4 will not be large enough to interfere with this idealized picture. The best known example of an undesirable effect from the other terms is, of course, the formation of "twin images" in classical holography[14] from the contribution of the A_3 term. Application of Barton's algorithm[4] to a monoenergetic photoelectron diffraction pattern results in twin images equal in magnitude to the true images of the atoms. Also, in the so-called "forward-scattering" geometry,[15] where scattering atoms are found between the reference-wave source and the detector, the strong forward-scattering nature of electron-scattering factors for electrons of energies greater than a few hundred eV gives rise to "forward-scattering peaks"[16] on the diffraction pattern in the regions of which the object waves $O(\mathbf{k})$ may be comparable with, or larger than, the reference wave $R(\mathbf{k})$. In such cases the contributions of the A_4 term above may even be dominant. These contributions give rise to the so-called "low-radius artifacts," discussed earlier in the literature.[7,17]

IV. APPLICATIONS OF THE LINEAR ALGORITHM

We illustrate the effects of these undesirable contributions by attempting to reconstruct the known positions of a small cluster of Si atoms surrounding a B photoemitter on a simple model of the Si(111)-$\sqrt{3}\times\sqrt{3}$ B surface, from its calculated photoelectron diffraction pattern. The unusual subsurface adsorption site of the B atoms and the accompanying $\sqrt{3}\times\sqrt{3}$ surface reconstruction of Si(111) can be realized experimentally by allowing B atoms to diffuse from the bulk to the surface from heavily B-doped Si samples. In our model, a B atom is assumed to be at a subsurface substitutional site in the second layer from the surface, directly beneath a Si atom, as shown in Fig. 1. There are five nearest-neighbor Si atoms around the B. In a photoelectron diffraction experiment with the B atom acting as an electron emitter, four of these atoms, termed Si(1)–Si(4), contribute to the diffraction pattern primarily as forward scatterers. The B-Si(1), B-Si(2), and

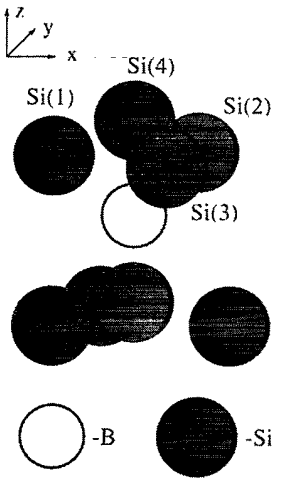

FIG. 1. Diagram of the cluster of near-neighbor atoms to a B atom on the Si(111)-$\sqrt{3}\times\sqrt{3}$ B surface. In this unusual adsorption site, the boron atom in the S_5 site is in the subsurface substitutional position in the second layer, directly underneath the Si(4) adatom.

B-Si(3) bond lengths are taken to be 2.15 Å, and the B-Si(4) length, 2.32 Å. The angle between any of the former set of bonds [e.g., B-Si(1)] and the B-Si(4) is taken to be 63°. The cluster has threefold rotation symmetry about the (111) surface normal. Also included in the cluster were the four near-neighbor atoms, shown in Fig. 1, below the B emitter. The adsorption site and near-neighbor bond lengths in our model were identical to those assumed by Tong *et al.* in their attempt to reconstruct the same geometry from a single calculated photoelectron diffraction pattern by their phase-shift correcting algorithm,[18] and from diffraction patterns of a range of several different electron energies by their small-window energy-extension process (SWEEP),[19] somewhat analogous to the multiple-wavelength Barton (10) or SWIFT (11) algorithms.

The photoelectron diffraction pattern resulting from a 500-eV electron emitted by the B atom and its subsequent full multiple scattering from all the atoms of the cluster (including the B emitter) was calculated by the concentric-shell photoelectron diffraction program of Saldin, Harp, and Chen.[20] We have assumed an *s*-wave emitter for simplicity. The result is shown in Fig. 2. The center of the pattern marks the projection of the (111) surface normal (the *z* direction indicated in Fig. 1), and the edge of the pattern corresponds to a 70° polar angle. The central peak on the diffraction pattern is due to the large object wave forward scattered by atom Si(4) of Fig. 1, while the similar dominant intensity features at the periphery of the pattern mark the forward-scattering features from atoms Si(1) to Si(3). Interference and multiple-scattering effects contribute to the weaker diffraction fringes also seen in the figure.

The difficulty of reconstructing from this diffraction pattern the positions of atoms Si(1) through Si(4) relative to the B emitter by means of an algorithm of the form (3) is illustrated in Figs. 3 and 4. The top panel in Fig. 3 shows the reconstructed radial image functions (RIF) (Ref. 21) in the surface-normal direction, corresponding to a polar angle of $\theta=0°$, connecting the B-atom source and the Si(4) atom. The lower panel in the same figure depicts the corresponding RIF along a line tilted away from the surface normal by $\theta=63°$, connecting the B source to, e.g., the Si(1) atom. Both RIF's were calculated by an algorithm of the form (3) using the Barton kernel (10). The vertical dashed line in the upper panel corresponds to the position of the Si(4) atom relative to the emitter (at the origin), while the similar dashed line in the lower panel marks the position of the Si(1) atom in our model. Note that, in both cases, a peak associated with the atom scatterer is found at a position displaced further away from the emitter than the true position of the

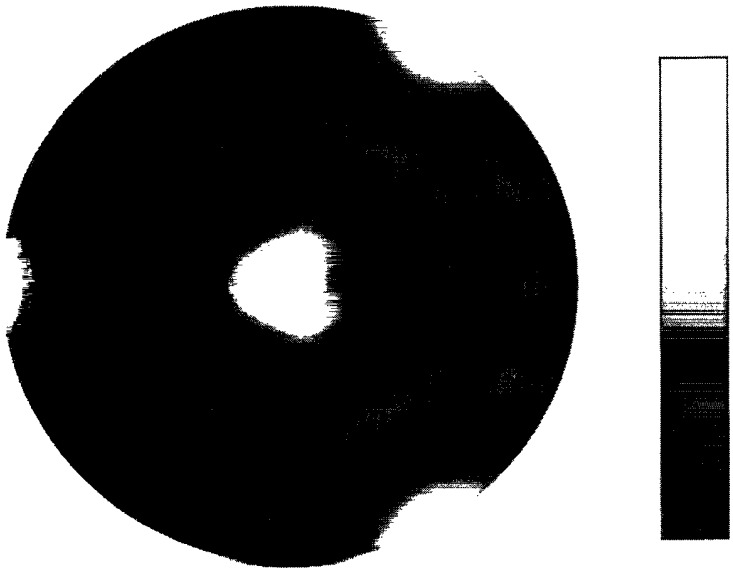

FIG. 2. Multiple-scattering calculation of the photoelectron diffraction from the *s*-wave B emitter and Si-atom scatterers of the atomic cluster of Fig. 1. The kinetic energy of the photoemitted electrons was taken to be 500 eV.

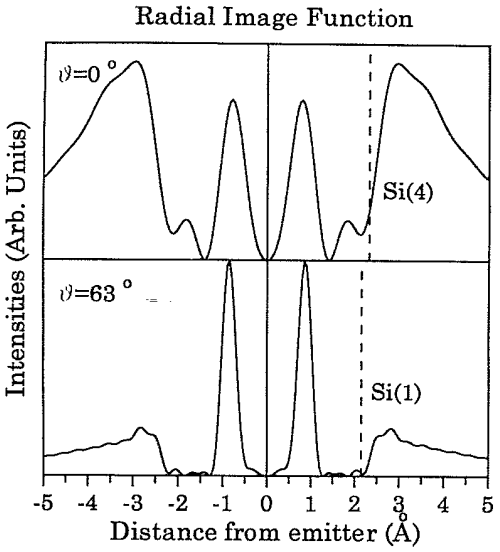

FIG. 3. Radial image functions (RIF's) reconstructed by an algorithm of form (3) and Barton's kernel (10) from the diffraction pattern of Fig. 2. The upper panel shows the reconstructed intensity along a line passing through the emitter and normal to the surface (with polar angle $\theta=0$), and the lower panel depicts the corresponding intensity along a straight line joining the emitter and the position of atom Si(1) of Fig. 1.

scatterer, consistent with the known properties of such an algorithm.[13,22] This peak shift has been shown[13,22] to be a consequence of the anisotropy of the atomic-scattering factor for an electron of such an energy. Also noticeable is the mirror symmetry of the RIF's about the origin, a feature consistent with the "twin images" of classical holography.[14,4] A third undesirable feature is the presence on these RIF's of strong intensity peaks around 1 Å from the source, which have no relation to any atom in our model. These are the so-called low-radius artifacts, discussed earlier in the literature.[7] They are a direct consequence of the existence of the strong forward-scattering peaks on the diffraction pattern of Fig. 2.

The results of repeating the calculation with the SWIFT kernel (11) replacing the Barton kernel (10) in the algorithm (3) are shown in Fig. 4. Here peaks are found almost exactly at the positions of the Si(4) and Si(1) atoms, on the RIF's in the directions of those atoms. It should be noted that the factor r in the numerator of the kernel (11) does appear to have removed the unsightly "low-radius artifacts," unlike an algorithm[18] which corrects only for the phase of the scattering factor. However, the presence of the factor r also increases the intensities at large radii on the RIF's to the extent that it is unclear *a priori* which of the peaks on the positive side of the $\theta=0$ RIF corresponds to the atom Si(4). Also troublesome is the fact that, although true mirror symmetry about the source atom has been removed, substantial intensities remain on the "twin" sides of the RIF's (corresponding to negative values of the abscissae on Fig. 4), a fact not conducive to the easy determination of a completely unknown structure from such a reconstruction.

It is the search for a more unambiguous reconstruction of the true atom positions from even a single diffraction pattern like that of Fig. 2 which leads us to the algorithm which we have named "atomic-position recovery by iterative optimization of reconstructed intensities," or APRIORI for short.[23] We describe this algorithm in Sec. V.

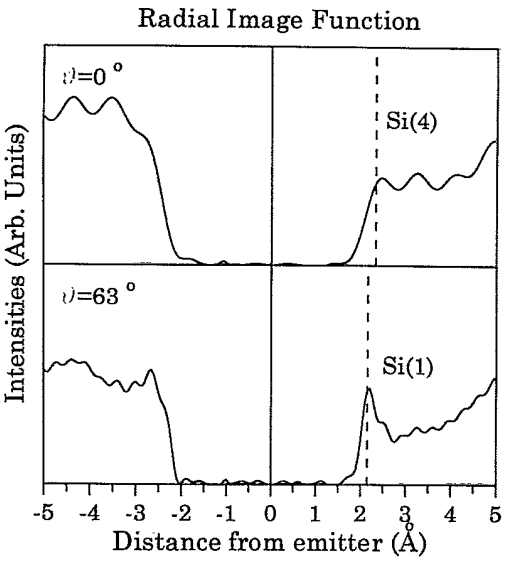

FIG. 4. Same as Fig. 3 except that the reconstructions were performed with the SWIFT kernel (11).

V. APRIORI—A NONLINEAR RECONSTRUCTION ALGORITHM

The results above show that an orthogonalization condition of the form (8) applied to the contribution $A_2(5)$ to (3) cannot always be relied upon to ensure that local intensity maxima corresponding to true atom positions at $\mathbf{r}=\mathbf{r}_i$ dominate contributions from the other terms A_1, A_3, and A_4. The term A_1 tends to produce a high-intensity region close to the emitter atom, and A_3 to the twin image.[22] The term A_4 arises from the squared object-wave term [the fourth term (1)] contributing to the intensity of a hologram. When the object-wave intensity is always much smaller than that of the reference wave, i.e., when

$$|O(\mathbf{k})| \ll |R(\mathbf{k})| , \tag{13}$$

A_4 is negligible compared with the other terms. In the case of the diffraction pattern of Fig. 2, however, this condition does not hold in the regions of the "forward-scattering peaks," as discussed in Sec. IV. Similar conclusions have been reached by Barton and Terminello.[24] It has been shown[7] that it is the dominant intensities of

the forward-scattering peaks which give rise to the low-radius artifacts on RIF's like those in Figs. 3 and 4.

An algorithm of the form (3) works best when the contribution to the reconstructed intensity from the term A_2 (5) is enhanced, while those from the terms A_1, A_3, and A_4 are reduced to smoothly varying background contributions. The results of Sec. IV show that, in practice, contributions to the hologram intensity from the first, third, and fourth terms in (1) can act to spoil an image of atom positions reconstructed by an algorithm of the form (3), even if a kernel could be found which satisfies an approximate orthogonality condition of the form (8). However, it should be noted that structural information is present even in the third and fourth terms of (1). Indeed, in a diffraction pattern like that of Fig. 2, the regions of highest intensity, and hence the best signal-to-noise ratio on experimental data, are in the forward-scattering peaks, which are dominated by the nonlinear object-wave terms. The philosophy of the APRIORI algorithm, which we describe below, is to use the information in all four of the terms in (1) contributing to the hologram intensity to recover relative atom positions.

The logic is the following: our aim is to recover the positions of nearby scattering atoms relative to the photoelectron sources, from the intensity distributions of a measured diffraction pattern. We are free to use any general physical information that we possess, such as the nature of the electron wave initially photoemitted from an atom (from calculated matrix elements of the *atomic* transition), and any knowledge of the chemical species (obtainable from a photoemission or Auger spectrum of the sample) and the core potentials of the scattering atoms. Fortunately, in the current practice of electron spectroscopies, such as low energy electron diffraction (LEED),[25] x-ray-absorption spectroscopy (XAS),[26] and photoelectron diffraction (PD),[15] these specifically *atomic* properties are decoupled from the *crystallographic* data of relative atom positions. We begin by defining a distribution $p_X(\mathbf{r}_i)$ (Ref. 27) of scattering atoms of chemical species X on a fine grid of positions $\mathbf{r}_i$ relative to the photoemitter. The theoretical expression for the far-field intensity, I_{th}, of a photoelectron diffraction pattern may be written in terms of this distribution, the reference wave $R(\mathbf{k})$, and the object wave $O_X(\mathbf{k},\mathbf{r}_i)$, scattered by an atom of chemical species X at a position $\mathbf{r}_i$ relative to the emitter.[23] The resulting expression is

$$I_{\text{th}}(\mathbf{k})=|R(\mathbf{k})|^2+\sum_{X,i}p_X(\mathbf{r}_i)M_X(\mathbf{k},\mathbf{r}_i)\ , \tag{14}$$

where

$$M_X(\mathbf{k},\mathbf{r}_i)=[R^*(\mathbf{k})O_X(\mathbf{k},\mathbf{r}_i)+\text{c.c.}]+O_X^*(\mathbf{k},\mathbf{r}_i)\sum_{Z,j}p_Z(\mathbf{r}_j)O_Z(\mathbf{k},\mathbf{r}_j)\ , \tag{15}$$

with c.c. representing complex conjugation, Z another dummy index for the chemical species of a scatterer atom, and $\mathbf{r}_j$ another point on the real-space grid.

If the emitter electron was initially in a state with azimuthal and magnetic quantum numbers l and m, the reference wave may be taken to be of the form

$$R(\mathbf{k})=Y_{lm}(\hat{\mathbf{k}})\ , \tag{16}$$

and the object wave arising from the scattering of this reference wave by an atom of chemical species X at position $\mathbf{r}_i$ may be written

$$O_X(\mathbf{k},\mathbf{r}_i)=Y_{lm}(\hat{\mathbf{r}}_i)\frac{f_X^{(l)}(\mathbf{k},\mathbf{r}_i)}{r}e^{(kr-\mathbf{k}\cdot\mathbf{r}_i)}\ , \tag{17}$$

where $f_X^{(l)}(\mathbf{k},\mathbf{r}_i)$ is the spherical-wave electron-scattering factor[13] of that atom.

Szöke[27] pointed out that if the usual holographic assumption (13) holds, the distributions $p_X(\mathbf{r}_i)$ may be recovered by solving the set of linear equations

$$|R(\mathbf{k})|^2+\sum_{X,i}p_X(\mathbf{r}_i)M_X(\mathbf{k},\mathbf{r}_i)=I_{\text{exp}}(\mathbf{k})\ , \tag{18}$$

which equate the theoretical estimates of the photoelectron intensities to experimental values of these quantities at different points on the diffraction pattern, since then the terms outside the square brackets in (15) may be neglected. He suggested that information about the scatterers contained in these distributions may be used to redefine the reference wave R, and the process repeated until the object waves really become negligible. Szöke[28] and Maalouf *et al.*[29] have applied an adaptation of this procedure to recover the electron density of a side chain of a macromolecule in a numerical simulation of a problem in x-ray crystallography.

We take a somewhat different approach. Due to experimental errors and limitations of the theoretical estimates of the experimental intensities, we attempt only to minimize the sum of the absolute errors

$$E(\mathbf{k})=|R(\mathbf{k})|^2+\sum_{X,i}p_X(\mathbf{r}_i)M_X(\mathbf{k},\mathbf{r}_i)-\mu I_{\text{exp}}(\mathbf{k}) \tag{19}$$

of the theoretical estimates of the measured intensities, where μ is a constant of proportionality to be determined. That is, we attempt to determine the distributions $p_X(\mathbf{r}_i)$ by minimizing

$$\sum_{\mathbf{k}}|E(\mathbf{k})|\ . \tag{20}$$

If condition (13) holds, the distributions $p_X(\mathbf{r}_i)$ may be conveniently determined by a linear programming technique.[30]

However, as we have pointed out earlier, in many problems, such as that of forward-scattering point-source electron diffraction, the nonlinear object-wave terms may be so large that condition (13) may not hold. Under such circumstances, an algorithm that assumes negligible object waves may not converge. On the other hand, if these terms, represented by the last term in (15), were retained, the problem becomes the much more difficult one of recovering $p_X(\mathbf{r}_i)$ by the minimization of a *nonlinear* function (19) of that distribution.

We solve this nonlinear problem by the following iterative procedure: at the nth iteration we determine the distribution $p_X^{(n)}(\mathbf{r}_i)$ which minimizes the sums of the absolute errors

$$\sum_{\mathbf{k}}|E^{(n)}(\mathbf{k})|\ , \tag{21}$$

where

$$E^{(n)}(\mathbf{k})=|R(\mathbf{k})|^2+\sum_{X,i}p_X^{(n)}(\mathbf{r}_i)M_X^{(n-1)}(\mathbf{k},\mathbf{r}_i) -\mu I_{\exp}(\mathbf{k}) , \quad (22)$$

with

$$M_X^{(n)}(\mathbf{k},\mathbf{r}_i)=[R^*(\mathbf{k})O_X(\mathbf{k},\mathbf{r}_i)+\text{c.c.}] +O_X^*(\mathbf{k},\mathbf{r}_i)\sum_{Z,j}p_Z^{(n-1)}(\mathbf{r}_j)O_Z(\mathbf{k},\mathbf{r}_j) , \quad (23)$$

a quantity which depends on the best estimate of the same distribution, $p_Z^{(n-1)}(\mathbf{r}_j)$ at the previous iteration. The procedure is somewhat analogous to the solutions of other nonlinear problems, such as the determination of a self-consistent wave function from a nonlinear Hartree or Hartree-Fock equation. The iteration cycles are initiated by arbitrarily choosing an initial distribution $p_Z^{(0)}(\mathbf{r}_j)$. We found that, for the photoelectron diffraction pattern in Fig. 2, containing strong forward-scattering peaks, the initial choice of

$$p_Z^{(0)}(\mathbf{r}_j)=\delta_{Z,X}\delta_{\mathbf{r}_j,\mathbf{r}_i} \quad (24)$$

gave the best results. This choice retains squared object-wave terms, but neglects cross terms between object waves due to scattering by different atoms, which have little overlap in the geometry of the particular cluster of atoms considered (Fig. 1).

Thus, at each iteration, the errors $E^{(n)}(\mathbf{k})$ are *linear* functions of the unknown distributions $p_X^{(n)}$, since the distributions $p_Z^{(n-1)}$ from the previous iteration are assumed to be known. At each iteration, the distributions $p_X^{(n)}$ and the value of the normalization constant μ, which minimize (21), subject to the constraints

$$0\le p_X^{(n)}(\mathbf{r}_i)\le 1 , \quad (25)$$

$$\sum_{\mathbf{r}_i}p_X^{(n)}(\mathbf{r}_i)=N_X \quad \text{for all } X \text{ and } \mathbf{r}_i , \quad (26)$$

and

$$\mu\ge 0 , \quad (27)$$

where N_X is the number of scattering atoms of type X, may be determined by a standard linear programming scheme.[30,31] An indication of the flexibility of a linear programming-based optimization scheme is that the constraint (26) is optional, and may be removed if the number of scattering atoms of each chemical species is not known beforehand. The iterations are repeated until self-consistency, i.e., until

$$p_X^{(n)}(\mathbf{r}_i)\simeq p_X^{(n-1)}(\mathbf{r}_i) . \quad (28)$$

The fact that spatial distributions $p_X(\mathbf{r}_i)$ are reconstructed simultaneously, but separately for each chemical species X enables the recovery of not only the positions of the scattering atoms, but their chemical identities.[23] In our earlier paper[23] we applied our algorithm to the determination of the positions of atoms forming a linear chain passing through an emitter. In this paper, we demonstrate that it is equally capable of accurately reconstructing the positions of a three-dimensional cluster of atoms surrounding an emitter.

VI. THREE-DIMENSIONAL RECONSTRUCTION BY THE APRIORI ALGORITHM

In this section we describe a practical implementation of the APRIORI algorithm to the reconstruction from the diffraction pattern of Fig. 2 of the spatial distribution $p_{\text{Si}}(\mathbf{r}_i)$ of the near-neighbor Si-atom scatterers relative to the B-atom emitter. Each iteration of the APRIORI algorithm was implemented by the revised simplex method of linear programming.[30] For the calculations reported in this paper we used the relevant subroutine from the IMSL Math Library. For our problem, the revised simplex method scales with computer time as[30]

$$(MN+2D)(D+N)^2 , \quad (29)$$

where M is the number of points on the spatial grid of p_{Si} values, N is the number of atomic species of the scatterers (in our case $N=1$), and D is the number of data points at which experiment/theory comparisons are made.

If the positions of the forward-scattering peaks on the diffraction pattern are assumed to be the projections of the directions from the emitter at which scatterers are found, a RIF like those of Figs. 3 and 4 may be reconstructed by defining a spatial distribution $p_{\text{Si}}(\mathbf{r}_i)$ of the Si-atom scatterers on a uniform grid of points along these directions only. The threefold rotation symmetry and mirror planes evident in the diffraction pattern of Fig. 2 indicate that independent data points are contained only within a symmetry-reduced 60° sector of the diffraction pattern. Both of these factors help to keep the magnitudes of M and D low enough to enable the rapid reconstruction of the radial image functions along the same directions as those of Figs. 3 and 4. The corresponding RIF's reconstructed by the APRIORI algorithm are shown in Fig. 5. Not only are the positions of the Si(1) and Si(4) atoms reconstructed extraordinarily accurately, but also there are no low-radius artifacts, or residual twin images, which marred the corresponding RIF's from the Barton and SWIFT algorithms in Figs. 3 and 4.

We may also attempt to recover the full three-dimensional (3D) distribution p_{Si} of the Si scatterers close to the B emitter. For this purpose we seek to determine the values of p_{Si} on a Cartesian grid of $33\times33\times33$ points along x, y, and z directions (defined on Fig. 1) in a $10\times10\times10$-Å^3 cube centered at the origin (the emitter position), corresponding to a grid spacing of 0.313 Å. In this case, the number of points, M on the spatial grid of p_{Si} values is as high as 35 937. The diffraction pattern of Fig. 2 is displayed from a dataset of about 12 868 data points arranged on a uniform Cartesian grid. Even allowing for the sixfold reduction due to symmetry, the number of independent diffraction data points was $D\simeq2145$. The application of the APRIORI algorithm, for such high values of M and D proved to be unacceptably time consuming on our computer. Since we did not wish to sacrifice spatial resolution on the reconstructed distribution p_{Si}, we employed a smaller subset of 64 data

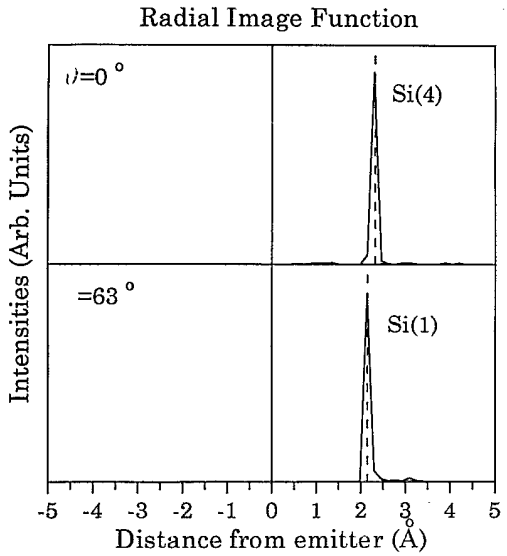

FIG. 5. Same as Fig. 3 except that the reconstructions were carried out by the APRIORI algorithm.

points for each run of the APRIORI algorithm. This yielded a self-consistent distribution $p_{Si}^{(4)}$ after four iterations of the algorithm. A different subset of 64 data points were next chosen to yield another distribution of $p_{Si}^{(4)}$, and the process continued until all data points of the diffraction pattern were utilized. The average of the resulting $p_{Si}^{(4)}$'s was taken as our final reconstructed distribution.

Two sections through the resulting 3D real-space grid of reconstructed intensities are shown in Fig. 6. The upper panel represents a section through this 3D array of intensities, passing through the origin (the position of the emitter atom, marked by a cross on this figure), and perpendicular to the y axis (y cut) in Fig. 1. This plane also cuts through the atoms Si(1) and Si(4) shown in Fig. 1. The bright reconstructed intensities in the upper panel of Fig. 6 are found at exactly the positions of these atoms in the model used to simulate the diffraction pattern of Fig. 2, and no hint of undesirable twin images is found. The lower panel in Fig. 6 represents the $z=0.96$ Å plane (z cut) through the reconstructed intensities. The bright intensities in this panel are likewise found exactly at the positions of the Si(1), Si(2), and Si(3) atoms in this plane.

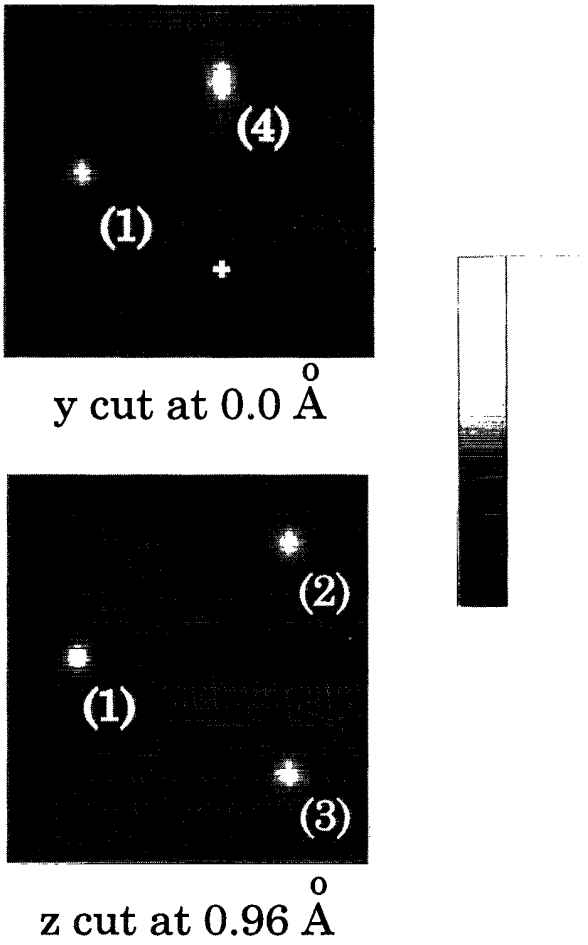

FIG. 6. Sections through the three-dimensional intensity distribution reconstructed by the APRIORI algorithm from the diffraction pattern of Fig. 2. Upper panel: Reconstructed intensity in the $y=0$ plane containing the positions of the emitter (denoted by the white cross) and those of the Si(1) and Si(4) scatterers, marked by spots of high intensity. Lower panel: Reconstructed intensity in the $z=0.96$-Å plane, where the positions of the Si(1), Si(2), and Si(3) atoms are also revealed by spots of high intensity.

VII. CONCLUSIONS

We have pointed out that many of the artifacts on the reconstructed "images" in holographic crystallography to date may be traced to the neglect of the nonlinear object-wave terms in the reconstruction algorithms. We have shown that these problems may be overcome by the nonlinear reconstruction scheme we call "atomic-position recovery by iterative optimization of reconstructed intensities" (APRIORI). We have demonstrated this by comparing our reconstruction, from a calculated diffraction pattern, of the positions of Si substrate atoms relative to a *subsurface* B-atom electron emitter on a Si(111)-$\sqrt{3}\times\sqrt{3}$ B surface, with those by linear reconstruction schemes. Unlike the linear prescriptions, which are known to have difficulties reconstructing an artifact-free image in such a "forward-scattering" geometry, the APRIORI algorithm is shown to be capable of recovering a very accurate and unambiguous real-space distribution of the positions of the scattering atoms from even a *single* diffraction pattern, with no hint of the undesirable twin images of classical holography.

ACKNOWLEDGMENTS

X.C. is grateful for financial support from the Graduate School and the Laboratory for Surface Studies of the University of Wisconsin-Milwaukee. D.K.S. acknowledges support for this work from the National Science Foundation (Grant No. DMR-9320275) and from the Donors of the Petroleum Research Fund, administered by the American Chemical Society.

[1]M. M. Woolfson, *Direct Methods in Crystallography* (Oxford University Press, Oxford, 1961).
[2]A. Szöke, in *Short Wavelength Coherent Radiation: Generation and Applications,* edited by D. J. Attwood and J. Boker, AIP Conf. Proc. No. 147 (AIP, New York, 1986).
[3]D. Gabor, Nature (London) **161,** 777 (1948).
[4]J. J. Barton, Phys. Rev. Lett. **61,** 1356 (1988).
[5]D. K. Saldin and P. L. De Andres, Phys. Rev. Lett. **64,** 1270 (1990).
[6]C. S. Fadley, Surf. Sci. Rep. **19,** 231 (1993).
[7]Z.-L. Han, S. Hardcastle, G. R. Harp, H. Li, X.-D. Wang, J. Zhang, and B. P. Tonner, Surf. Sci. **258,** 313 (1991).
[8]J. J. Barton and L. J. Terminello, *The Structure of Surfaces III,* edited by S. Y. Tong *et al.* (Springer, Berlin, 1991); S. Y. Tong, H. Li, and H. Huang, Phys. Rev. Lett. **67,** 3102 (1991); J. J. Barton, *ibid.* **67,** 3106 (1991); L. J. Terminello, J. J. Barton, and D. A. Lapiano-Smith, *ibid.* **70,** 599 (1993); J. G. Tobin *et al., ibid.* **70,** 4150 (1993); H. Wu *et al., ibid.* **71,** 251 (1993); K.-M. Schindler *et al., ibid.* **71,** 2054 (1993); C. S. Fadley *et al.,* J. Electron Spectrosc. **68,** 19 (1994).
[9]M. A. Mendez, C. Gluck, and K. Heinz, J. Phys. Condens. Matter **4,** 999 (1992).
[10]C.-M.Wei and S. Y. Tong, Surf. Sci. **274,** L577 (1992); C.-M. Wei *et al.,* Phys. Rev. Lett. **72,** 2434 (1994).
[11]P. Hu and D. A. King, Nature **360,** 656 (1992).
[12]J. B. Pendry and D. K. Saldin, Surf. Sci. **145,** 33 (1984); K. Heinz, D. K. Saldin, and J. B. Pendry, Phys. Rev. Lett. **55,** 2312 (1985).
[13]B. P. Tonner, Z.-L. Han, G. R. Harp, and D. K. Saldin, Phys. Rev. B **43,** 14 423 (1991).
[14]R. J. Collier, C. B. Burckhardt, and L. H. Lin, *Optical Holography* (Academic, New York, 1971).
[15]For a recent review, see, e.g., S. A. Chambers, Surf. Sci. Rep. **16,** 263 (1992).
[16]X. Chen, G. R. Harp, and D. K. Saldin, J. Vac. Sci. Technol. A **12,** 428 (1994).
[17]S. Hardcastle, Z.-L. Han, G. R. Harp, J. Zhang, B. L. Chen, D. K. Saldin, and B. P. Tonner, Surf. Sci. **245,** L190 (1991).
[18]S. Y. Tong, C. M.Wei, T. C. Zhao, H. Huang, and Hua Li, Phys. Rev. Lett. **66,** 60 (1991).
[19]S. Y Tong, Hua Li, and H. Huang, Phys. Rev. Lett. **67,** 3102 (1991).
[20]D. K. Saldin, G. R. Harp, and X. Chen, Phys. Rev. B **48,** 8234 (1993).
[21]G. R. Harp, D. K. Saldin, and B. P. Tonner, Phys. Rev. B **42,** 9199 (1990).
[22]D. K. Saldin, G. R. Harp, B.-L. Chen, and B. P. Tonner, Phys. Rev. B **44,** 2480 (1991).
[23]D. K.Saldin, X. Chen, N. C. Kothari, and M. H. Patel, Phys. Rev. Lett. **70,** 1112 (1993).
[24]J. J. Barton and L. J. Terminello, Phys. Rev. B **46,** 13548 (1992).
[25]M. A. Van Hove, W. H. Weinberg, and C.-M. Chan, *Low Energy Electron Diffraction* (Springer-Verlag, Berlin, 1986).
[26]See, e.g., *Principles, Applications, Techniques of EXAFS, SEXAFS, and XANES,* edited by D. C. Koningsberger and R. Prins (Wiley, New York, 1988).
[27]A. Szöke, Phys. Rev. B **47,** 14 044 (1993).
[28]A. Szöke, Acta Crystallogr. Sect. A **49,** 853 (1993).
[29]G. J. Maalouf, J. C. Hoch, A. S. Stern, H. Szöke, and A. Szöke, Acta Crystallogr. Sect. A **49,** 866 (1993).
[30]M. S. Bazaraa, J. J. Jarvis, and H. D. Sherali, *Linear Programming and Network Flows* (Wiley, New York, 1990).
[31]See, e.g., W. H. Press, S. A. Teukolsky, W. T. Vetterling, and B. P. Flannery, *Numerical Recipes: The Art of Scientific Computing* (Cambridge University Press, Cambridge, 1986).